Applied Acoustics 122 (2017) 23–34

Contents lists available at ScienceDirect

Applied Acoustics

journal homepage: www.elsevier.com/locate/apacoust

An ultrasonic guided wave approach for the inspection of overhead transmission line cables

Mehmet K. Yücel [a,b,*], Mathew Legg [a,c], Vassilios Kappatos [a,d], Tat-Hean Gan [a]

[a] Brunel Innovation Centre, Brunel University, Uxbridge, Middlesex UB8 3PH, United Kingdom
[b] STM Defense Technologies Engineering and Trade Inc., Ankara, Turkey
[c] School of Engineering & Advanced Technology, Massey University, Auckland, New Zealand
[d] Department of Technology and Innovation (ITI), University of Southern Denmark (SDU), Campusvej 55, DK-5230 Odense M, Denmark

ARTICLE INFO

Article history:
Received 26 September 2016
Received in revised form 5 February 2017
Accepted 7 February 2017

Keywords:
Ultrasonic guided waves
ACSR cables
Overhead transmission line cables
Wavelet transform
Multi-wire cables
Non-destructive testing

ABSTRACT

Inspection of overhead transmission line cables is performed using various non-destructive testing techniques, such as visual, temperature, and eddy current-based inspection; yet each of these techniques have their respective shortcomings and safety concerns. The use of ultrasonic guided waves as a non-destructive testing technique is well established for simple geometries such as plates, pipes, and rods. However, its application for multi-wire cables is still in development. In this study, ultrasonic guided waves excited by a shear mode transducer collar are utilised as a defect detection technique for untensioned aluminium conductor steel reinforced cable specimens. The identification and analysis of wave propagation for a broad range of frequencies is performed using a laser scanning vibrometer, and the effect of defect size on wave propagation is studied. Signal processing algorithms, such as wavelet denoising and time scaling, are then deployed for inspection quality enhancement and analysis under noisy conditions. Results yield an extended range of defect detection coverage in pulse echo configuration; with successful detection of defects that correspond to a 4.5% reduction in the cable's cross sectional area; and up to 24% improvement of signal-to-noise ratio.

1. Introduction

Multi-wire cables are extensively used in a broad spectrum of engineering applications to meet various demands; such as load carrying in bridges, cranes, and elevators; post-tensioning in concrete structures; and electricity transfer in power grids. Overhead Transmission Line (OVTL) cables span long distances and form the backbone of the energy distribution grid. Throughout their service life time, OVTL cables are influenced by various effects such as operational factors (applied tensile stress and voltage stress) and environmental factors (wind-induced vibrations, icing, melting, and lightning strikes). Those factors, especially if the specimen has structural imperfections due to faulty manufacturing, can result in structural failures such as broken insulators, loose earth conductors, mechanical failures (twisted/ruptured/broken wires), and corrosion [6,29]. Structural failures have been reported to start emerging in the aluminium layers first [2]. In some cases, however, the steel core is reported to be intact even though the aluminium layers had structural failures [6]. The consequences of a structural failure in OVTL cables is reported in [2], where the failure of Aluminium Conductor Steel Reinforced (ACSR) cables left 67 million people under a power blackout in Brazil. Therefore, a reliable and fast inspection system, preferably an automated one with minimum human involvement, is desirable.

Certain Non-destructive Testing (NDT) techniques have emerged and have been widely used to provide pre-emptive measures against structural failures. Airborne and on-ground visual inspection performed by trained personnel is one of the first methods devised for structural maintenance of OVTL cables. It requires extensive care from personnel [28] and it is subject to regulations [31]. Manual visual inspection, however, is time-consuming, prone to human errors and has associated health hazards; primarily for airborne inspections where helicopter crashes have resulted in loss of lives [12]. In order to avoid human error and reduce health hazards, recent inspection methods have used different techniques to automate inspection systems. Automated visual inspection systems have been developed which apply image processing algorithms on videos/images acquired by either installed camera systems or airborne image acquisition systems. The efficiency of those methods relies heavily on the quality of the acquired images, and thus on the quality of the camera and the stability of the aerial

* Corresponding author at: Brunel Innovation Centre, Brunel University, Uxbridge, Middlesex UB8 3PH, United Kingdom.
E-mail addresses: mkerimyucel@gmail.com (M.K. Yücel), m.legg@massey.ac.nz (M. Legg), vk@iti.sdu.dk (V. Kappatos), tat-heangan@brunel.ac.uk (T.-H. Gan).

http://dx.doi.org/10.1016/j.apacoust.2017.02.003
0003-682X/

vehicle [15]. Temperature inspection methods have been proposed in [30,32], where infrared cameras were used to collect images of the power line components to detect corona effects triggered by structural discontinuities. Eddy current-based systems for the inspection of OVTL cables are reported in [16,34], where eddy currents are utilised for the detection of broken strands and corrosion on an OVTL cable. Kasinathan et al. has described the utilisation of fibre optic cables for temperature monitoring of OVTL cables to extract structural integrity information [14]. Radio and audible noise monitoring to acquire structural health information has also been proposed for OVTL cables [22]. In order to increase inspection range and quality, some studies have also utilised advances in robotics for the inspection of OVTL cables. The use of robotics, however, has its respective disadvantages, such as complexity in design, maintenance of robots, electromagnetic interference to communication systems of remote controlled robots, optimisation of weight and line tracking abilities for unmanned aerial vehicles [15]. In order to tackle design complexity, human errors, and health hazards associated with the abovementioned methods, Ultrasonic Guided Wave (UGW) based NDT methods have been investigated.

UGW based NDT techniques have been utilized for the interrogation of various multi-wire cable structures, and studies related to guided wave characterisation and defect detection in multi-wire cables have emerged. Xu et al. utilised magnetostrictive transducers to generate UGW for defect detection in seven-wire steel prestressing cables [13], and also investigated guided wave-based defect detection of 31 and 37-wire stay cables [35]. Liu et al. studied the optimisation of magnetostrictive transducer configuration to enhance guided wave inspection quality [20]. Studies have also emerged focusing on the possible effects of various factors that affect the wave propagation in multi-wire cables. Rizzo et al. studied ultrasonic wave propagation in seven-wire steel strands and analysed the changes in wave propagation with progressive loads applied on the cable [25]. Liu et al. also analysed the effects of temperature on wave propagation in multi-wire steel strands and related the wave propagation velocity variations to temperature changes [19]. The emphasis was also given to ACSR cables in several UGW based NDT studies. Haag et al. investigated guided wave propagation in ACSR cables with the aim of understanding energy transfer between wires, and formulated a computationally efficient energy-based model to predict the wave propagation in a simplified two-rod system with friction contact [9]. Branham et al. reported the feasibility of defect detection in ACSR cables with two different transducer coupling schemes and an understanding of attenuation and dispersion in ACSR cables [5]. Gaul et al. reported an overall feasibility analysis of the use of guided waves for damage detection in ACSR cables with an emphasis on the reflection of wave packets at structural discontinuities with varying geometry and size [8]. In one of the latest studies, Baltazar et al. investigated the changes in guided wave propagation in ACSR cables in the presence of a defect, and reported that the energy of the flexural modes changes when a defect is introduced and this change can be monitored for defect detection [3]. However, the abovementioned studies have not investigated the inspection efficiency for long OVTL cables under noisy (i.e. measurement noise, random noise, etc.) conditions.

The detection of defects in noisy environments, spatially overlapping echoes coming from closely spaced defects and the effects of dispersion phenomenon on wave propagation in interrogated media have been problematic for UGW applications, and raised the necessity of signal processing methods for inspection quality enhancement. Time-frequency analysis, deconvolution-based approaches, split spectrum processing, pulse compression [11], sparse signal representations, empirical mode decomposition [36], frequency warping [21] and wavelet transforms have been used for ultrasonic NDT applications [37]. Various studies have reported the use of advanced signal processing algorithms for the analysis of wave propagation and defect detection for multi-wire cables. Rizzo et al. utilised Discrete Wavelet Transform (DWT) to extract wavelet domain features for enhanced defect characterisation in multi-wire strand structures [27], and also reported the strength of DWT-based denoising in defect detection [26]. The wavelet transform has also been utilised to achieve good time-frequency representation quality for defect detection in ACSR cables, as reported by Salazar et al. in [10].

The design of a reliable and efficient NDT system requires thorough understanding of the wave propagation in the medium of concern. Evaluation of transducer coupling and respective analysis of wave propagation should be performed to achieve optimal results. In reference [17], the authors presented a study on the use of dispersion compensation for increasing the inspection range for ACSR cables using UGW. To accomplish this, the wave propagation on an untensioned 26.5 meter long Bear 325 ACSR cable was investigated. It was found that the UGW signal consisted of a single wave mode, the longitudinal $L(0,1)$ wave mode, which propagated along individual outer aluminium wires of the cable. While this gave good understanding of the wave propagation over long lengths of cable, it did not investigate wave propagation for short lengths of the cable or across the cable's cross section.

The current paper builds on the work presented in reference [17] by investigating the wave propagation on shorter lengths of untensioned cable and also across the cross section of the cable. In addition to this, the effects on the UGW signal of adding masses and different depth cuts to the cable are investigated. Following this, improved localisation of defects using wavelet de-noising is investigated. Section 2 provides information about the cable and the hardware used in this work. Section 3 presents the experimental set up and necessary theoretical information for wave propagation characterisation. The effect of adding masses and introducing defects is investigated in Section 4. The results of wavelet denoising and time scaling algorithms applied to the experimental results are presented in Section 5. Section 6 provides a discussion on some limitations of this work and areas for future research. Finally, a conclusion is provided in Section 7.

2. Experimental procedure

2.1. Cable information

ACSR cables are among the most widely used power transmission line cables. They are made of twisted aluminium and steel wires. The diameter of the individual wires and number of wires forming the cable vary between different ACSR cables. The cable used in this study, which has the codename Bear 325, has an overall diameter of 23.45 mm and consists of an inner core composed of seven steel wires, which are covered in anti-corrosive grease,

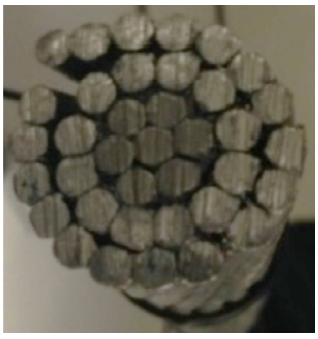

Fig. 1. Photo of cable cross section.

Table 1
Cable information.

Material	No. layers	Wire diameter [mm]	Number of wires	Other features
Steel	1	3.4	7	Core diameter: 10.05 mm
Aluminium	2	3.4	Inner layer: 12 Outer layer: 18	Surface pitch: 300 mm

and two outer layers of 12 and 18 aluminium wires respectively. Fig. 1 illustrates the cross sectional of the cable. The wire strands are twisted into a helical shape with each layer being twisted in the opposite direction.

Measurements where made using two different lengths (2 m and 26.5 m) of ACSR cables, which were not under tension. These specimens have the same structural properties (diameter, material, pitch, wire configuration, etc.). Table 1 provides information with regards to the structure of the cable under investigation.

2.2. NDT hardware

The transducer collar that was designed and manufactured for this study is illustrated in Fig. 2(a). The collar consists of six shear-mode Lead Zirconate Titanate (PZT) broadband transducers with sufficiently flat response in the frequency range of concern (up to 500 kHz). These transducers were aligned to excite vibration in the longitudinal direction of the cable. Since these were shear transducers, no coupling agent was used. Instead springs were used to push the transducers against a thin sheet of aluminium that was wrapped around the cable. The spring force used was not measured.

The transducer collar was connected to a Teletest Focus [23], a commercially available Long Range Ultrasonic Testing (LRUT) system. A 1 MHz sampling frequency was used for both Transmit (TX) and Receive (RX). The resulting acquired data was then transferred to a computer for analysis and post-processing in MATLAB. The time window used for measurements ranged from about 2 to 55 ms depending on the length of the cable and the number of echoes from the end of the cable that were being used for analysis. Power gain levels varied with experiments; 20 dB for Laser Scanning Vibrometer (LSV) experiments and 37 dB for defect detection experiments. The signals used for driving the transducers ranged from broadband pulses to Hann-windowed 10-cycle tone burst signals with different centre frequencies ranging from 20 to 400 kHz.

A PSV-400 PolyTec LSV[1] was used to measure the signal propagating along a 2 m long ACSR cable specimen. This was a 3D vibrometer which allowed the vibration in three dimensions to be measured. To improve the signal measured by the vibrometer, the cables were treated by coating them with reflective powder. The transducers were driven with a range of transmit signals. The resulting signals were sampled at evenly spaced scan points on the surface of the cable. Three types of scan grids were used in this work, see Fig. 3. The number of scan points was optimised in the scan area to have appropriate resolution. LSV measurements were repeated 70 times at each scan point and were averaged to improve the Signal-to-Noise Ratio (SNR).

3. Characterisation of wave propagation

In order to achieve optimal defect detection and localisation using UGW, characterisation of the wave propagation in the structure of interest is necessary. In this context, since aluminium layer inspection is emphasised, identification of the optimal excitation frequency for energy concentration in the aluminium layers is important. Moreover, for accurate defect localisation, the UGW modes propagating along the cable must be identified and their respective group velocity dispersion curves calculated. In this section, the abovementioned information is sought using LSV experiments.

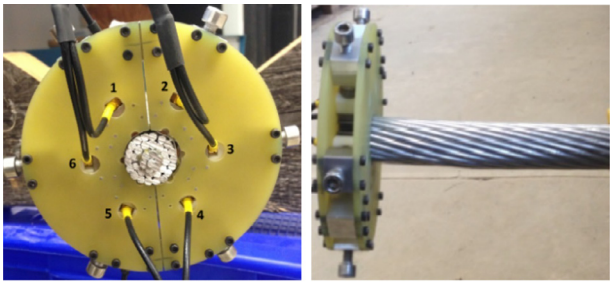

Fig. 2. Photos of the transducer collar which contained six shear mode PZT transducers that were mounted around the circumference of the cable.

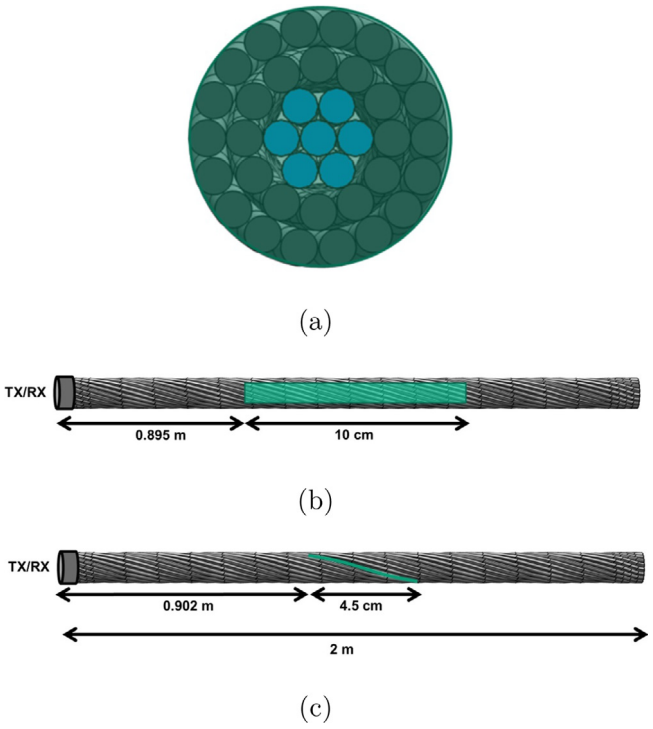

Fig. 3. Diagram illustrating the geometry of the LSV scan grid (a) on the end of the cable (both steel and aluminium layers), (b) a rectangular grid on the side of the cable covering multiple wires, and (c) a line scan along an individual wire.

3.1. End of cable LSV scan measurement

The first LSV scan was performed on the end of the two meter long cable, see Fig. 3(a). This was performed to investigate the optimal excitation frequency for the hardware used and the penetration of the signal through the cross section of the cable.

[1] http://www.polytec.com/products/vibration-sensors/scanning-vibrometers/.

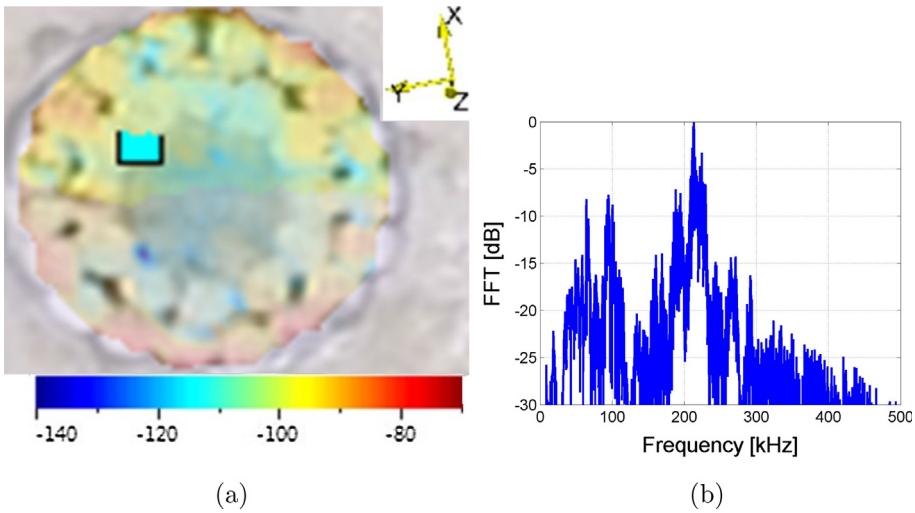

Fig. 4. Image (a) shows a LSV velocity map in dB (0 dB is 1 m/s) for vibration of the wires in the *Z* axis direct at the end of the cable for broadband MLS excitation. Plots (b) show the velocity FFT for a single scan point in the aluminium layer (shown as a blue rectangle).

Transducers were driven with a broadband (up to 500 kHz) Maximum Length Sequence (MLS)[2] pulse excitation signal. The resulting signals measured across the end of the cable were analysed using LSV software and MATLAB. Fig. 4(a) shows a velocity map obtained for all scan points for a single frequency. This map shows that for this frequency the wave energy is strongest in the aluminium layers.

Fig. 4(b) shows the velocity Fast Fourier Transform (FFT) obtained from the signal measured at a single a scan point in an aluminium layer. It can be seen that wave energy is high for the frequency range between 200 and 300 kHz. For this hardware, this frequency range would appear to be optimal for UGW testing of this cable. However, it should be noted that this frequency dependant gain may be related to the gain of the pulser-receiver hardware. Future work should investigate this frequency dependant gain in more detail.

3.2. Wave mode identification

The presence of wave modes and the dynamics of wave propagation on the outer wires was investigated using LSV scans on the side of the cable. A rectangular scan grid was used. The transducers were excited with Hann-windowed 10-cycle tone burst excitation signals for a range of frequencies and also a broadband MLS pulse.

Fig. 5 shows LSV 3D velocity maps for 20, 125, and 250 kHz excitation, while Fig. 6 provides plots of the corresponding velocity time traces for a single scan point. It can be seen that the 250 kHz excitation frequency resulted in larger amplitude signals than those obtained for 20 or 125 kHz. This result correlates with the results from Fig. 4(b). Fig. 5 also shows that the ultrasonic waves tend to propagate along individual wires, though some limited transfer of energy between wires could be seen. It may be that the wires with higher amplitude signal were those in direct contact with transducers. However, this was not confirmed experimentally at the time by following the individual wires back to the transducers.

The propagation of the wave through individual wires rather than the cable as a whole means that the ultrasonic velocity of the ultrasonic waves along the cables length will be lower than that along individual wires. For a cable with a length $L = Nt$, the

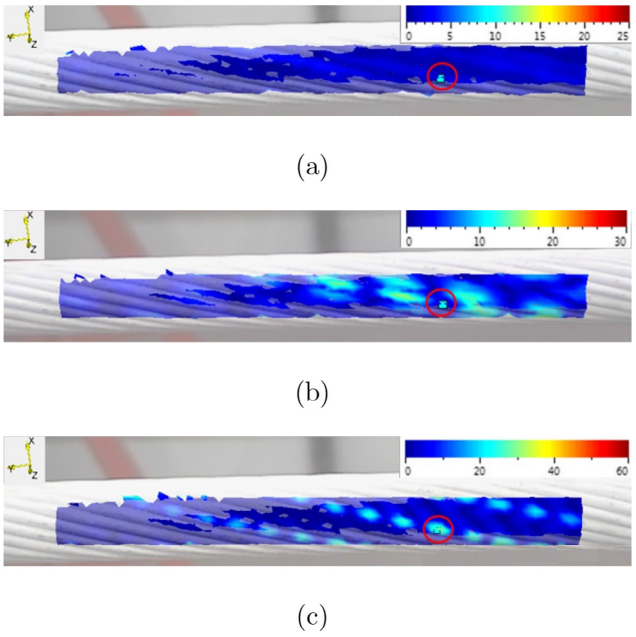

Fig. 5. LSV 3D-velocity values in dB for transmit frequencies of (a) 20 kHz, (b) 125 kHz, and (c) 250 kHz at the times when each signals' velocity value was at its peak.

actual distance travelled by the waves, the helical length, may be calculated using

$$L_{Helical} = N\sqrt{4\pi^2 d^2 + t^2} \quad (1)$$

where N is the number of turns, t is the pitch, and d is the diameter of the helix. From here onwards, time-of-arrival calculations are calculated with the helical length correction taken into account.

3.2.1. Analysis of wave propagation using short time Fourier transforms

Investigation of the wave modes propagating along the cable was performed using LSV measurement of the signal resulting from a broadband (up to 500 kHz) MLS pulse transmit signal. Fig. 7 shows Short Time Fourier Transform (STFT) (spectrogram)

[2] https://au.mathworks.com/matlabcentral/fileexchange/22716-kasami-sequences–m-sequences–linear-feedback-shift-registers.

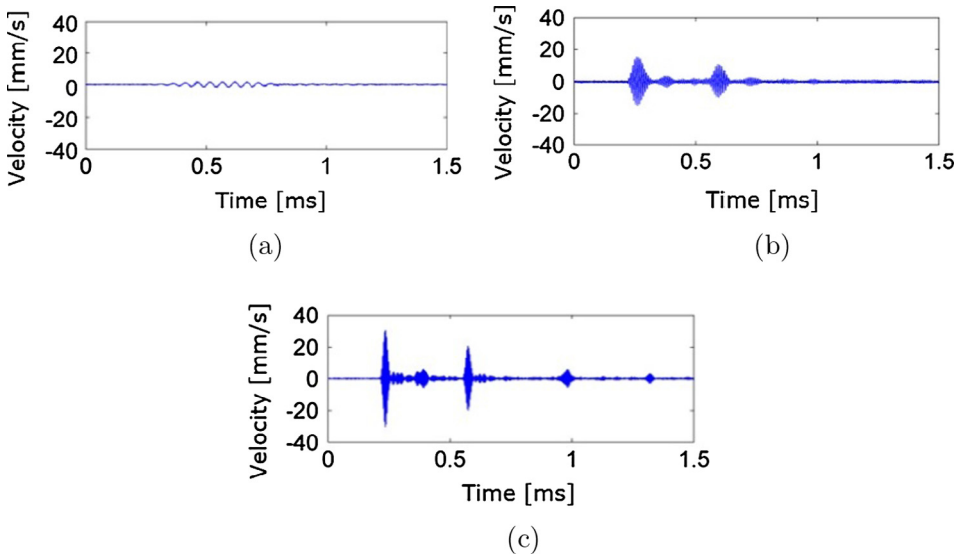

Fig. 6. Graphs of the LSV measured velocities, for the circled point on the cable shown in Fig. 5, in the *Y* axis direction for (a) 20 kHz, (b) 125 kHz, and (c) 250 kHz.

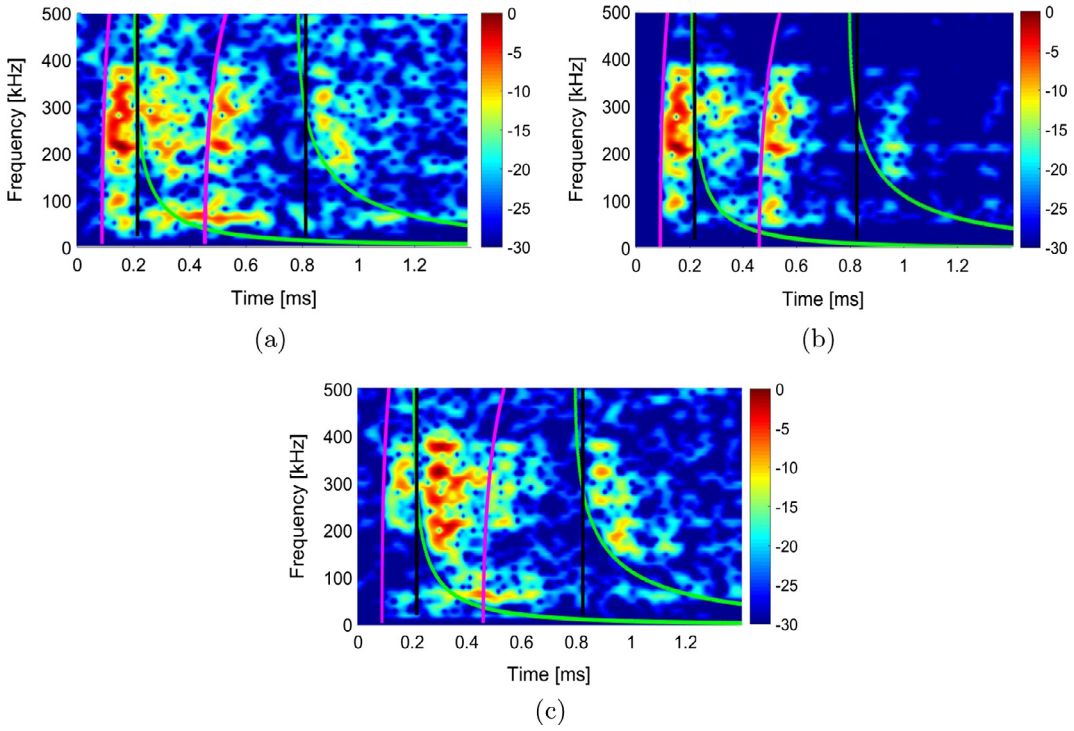

Fig. 7. Graphs show the Short-Time Fourier Transform of the energy velocity for broadband MLS pulse excitation with theoretical arrival time curves for aluminium wires overlaid for; (magenta line) direct arrival and first echo of L(0,1), (black line) T(0,1), and (green line) F(1,1) in the (a) *X*, (b) *Y*, and (c) *Z* axes directions. (For interpretation of the references to colour in this figure legend, the reader is referred to the web version of this article.)

representations of the velocity time trace for the circled vibrometer scan point shown in Fig. 5. Overlaid are theoretical arrival time curves calculated using the group velocity dispersion curves for the single wire case obtained using Disperse[3] software.

The velocity values show that four distinguishable wave packets are received by the vibrometer. The first wave packet appears to be the fundamental longitudinal wave mode. The second wave packet could be the torsional or flexural wave mode since both modes have similar theoretical arrival times. Nevertheless, the second wave packet appears to be the flexural mode since the lower frequency region (<100 kHz) of the second wave packet approximately follows the theoretical arrival time curve of the flexural wave mode. The third and fourth wave packets also appear to follow the fundamental longitudinal and flexural modes' theoretical arrival time curves. However, in the *Y* axis direction, the flexural wave mode appears to have been more strongly attenuated and another echo of the longitudinal wave mode is apparent.

The received wave packets have their energy spread over the spectrum, mainly between 50 and 400 kHz. The most powerful frequency component in the spectrum is also observed to be between

[3] http://www.imperial.ac.uk/non-destructive-evaluation/products-and-services/disperse/.

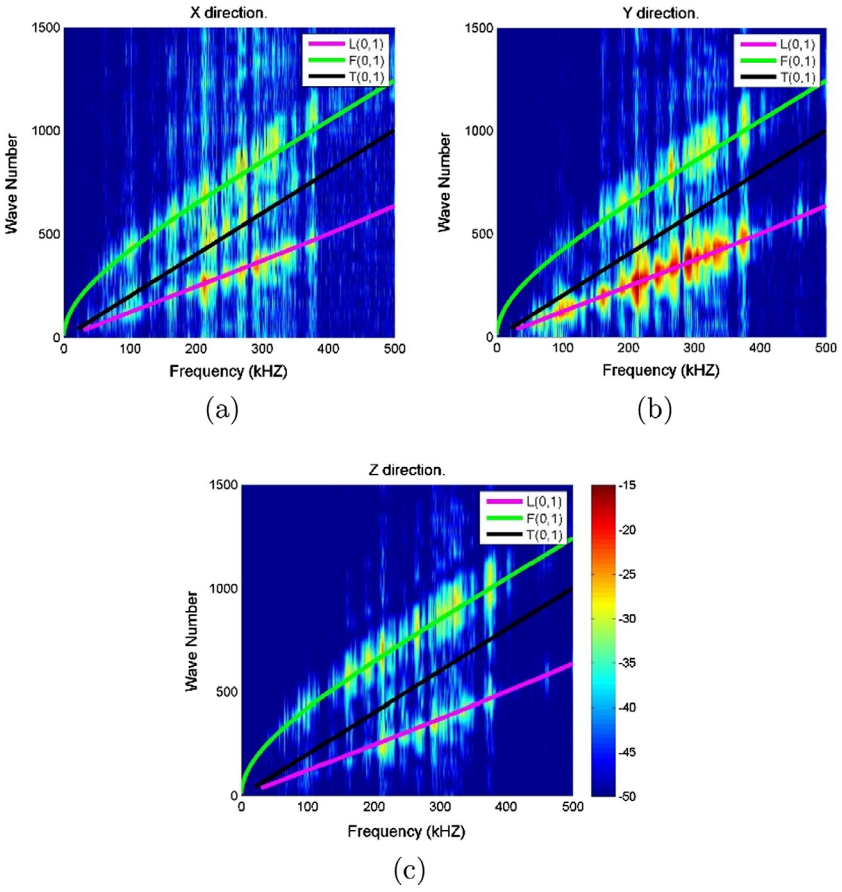

Fig. 8. Experimentally measured dispersion curves in the wave number frequency domain for the (a) *X*, (b) *Y* and (c) *Z* directions. Overlaid are the theoretical dispersion curves, for aluminium rods of the same diameter as the wires, which were calculated using Disperse software.

200 and 300 kHz. The flexural wave mode is attenuated more than the longitudinal mode. Therefore, in contrast with the findings of [3], the longitudinal mode is more appropriate for defect detection.

3.2.2. Wave number frequency domain analysis of wave propagation

The previous section provided an indication of the wave modes which were propagating along the 2 meter long cable. However, a more quantitative analysis was required. Therefore, the dispersion curves were experimentally measured using the 2D Fourier Transform technique presented by Alleyne and Cawley [1]. Since the ultrasonic waves propagate through individual aluminium wires, a LSV line scan was made along a single wire using evenly spaced scan points, see Fig. 3(c). The transducers were excited with a broadband MLS pulse (up to 500 kHz) excitation signal. The resulting signal measured at each point was used to create a time-distance domain matrix where the n^{th} row consisted of the signal measured at the n^{th} scan point. This was converted to the wave number-frequency domain using a two dimensional Fast Fourier Transform (2D-FFT). The resulting matrix was plotted as a 2D image, see Fig. 8 (colored data).[4] This provides experimental measurement of the dispersion curves. Overlaid over this are the theoretical wave number dispersion curves for a single aluminium wire. These were obtained by converting the single wire phase velocity V_{ph} dispersion curves to wave numbers k using

$$k = \frac{\omega}{V_{ph}}, \tag{2}$$

where ω is the angular frequency.

Fig. 8 shows good agreement between the theoretical dispersion curves for a single aluminium wire and the experimentally measured curves. Moreover, Figs. 8 and 7 show that the fundamental longitudinal mode is the most pronounced mode, whereas the fundamental torsional is non-existent except in the X-direction. The fundamental flexural mode is received, though it is more attenuative and dispersive. Therefore, the fundamental longitudinal mode is the best wave mode for defect detection. From here onwards, only the fundamental longitudinal mode excitation is considered.

4. Added mass and defect detection analysis

UGW-based NDT systems are able to detect defects because reflections of ultrasonic guided waves occur when they encounter a structural discontinuity. Structural discontinuities can exist in different forms. In cylindrical structures, structural discontinuities lead to changes in Cross Sectional Area (CSA), either positive or negative. This could take the form of masses added to the cable or reduced mass in the form of corrosion or broken cables. The following two sections describe experiments performed looking at the effect of changing the CSA on UGW by adding masses and a cut to the cable.

4.1. Masses attached to the cable

Reflections of UGW occur when they encounter changes in CSA. Therefore, adding masses to a cable allows defects to be simulated at different locations on the cable without damaging the cable. This

[4] For interpretation of color in Fig. 8, the reader is referred to the web version of this article.

is in contrast to a cut, which is permanent. Adding masses also allowed the effect of different structures such as spacers to be investigated. Spacers are structures which are used to separate groups of cables at regular intervals along a cable span.

The signals received when attaching masses to a cable was investigated using a 26.5 m long ACSR cable in pulse-echo configuration. Individual aluminium wires were cut from another cable specimen and attached around the circumference of the cable and tightened with a clip, as illustrated in Fig. 9(a). The cross section of the cable was approximately doubled by adding this mass, though the exact amount added was not measured. Initially a single set of aluminium wires were attached 23 m from the transducer collar. Afterwards, a second set of aluminium wires were attached 5.5 m from the transducer collar. A representative diagram of this experimental setup is shown in Fig. 9(b). The excitation signal used to drive the transducers was a Hann-windowed 10-cycle single tone burst excitation. A frequency sweep was then performed between 20 and 350 kHz to find the best frequency for UGW testing.

Fig. 10(a) shows the time domain representation for 220 kHz signal with one set of masses attached. Echoes from the mass and the cable end are visible. The Root Mean Square (RMS) values of the echoes that were reflected from the masses were acquired for various frequencies. These were obtained using a fixed-sized window, which was used to localise and calculate the RMS values of the echoes. For different frequencies, the window was shifted to allow for the change in group velocity of the longitudinal wave mode with frequency. Fig. 10(b) shows RMS values vs. frequency for one set of masses attached around the cable. In line with the LSV analysis results, the RMS peak is observed to be between 200 and 300 kHz, and the peak is located at 220 kHz.

Fig. 10(c) shows an example of the time domain signal for two masses attached to the cable. The corresponding RMS values for each mass echo vs. frequency are shown in Fig. 10(d). The echo from the first mass (located 5.5 m from the transducers) has a higher RMS value due to its proximity to the transducers whereas the echo coming from the second mass has a lower RMS value. Both RMS values have their peaks between 200 and 300 kHz, which is similar to the results for only one mass attached to the cable. The RMS peaks of the two mass echoes are not at the same frequency. The echo from the first mass peaks at 250 kHz whereas the echo from the second mass peaks at 240 kHz.

The resolution of defect detection (the minimum distance that two defects can be separated and still be resolved in the signal) was investigated and found to be approximately 1.5 m. This distance was used in the following section when deciding where to put a cut in the cable for real defect detection analysis.

4.2. Saw cut in the cable

A defect was introduced into the cable in the form of a transverse saw cut. This cut was machined into the cable at a distance

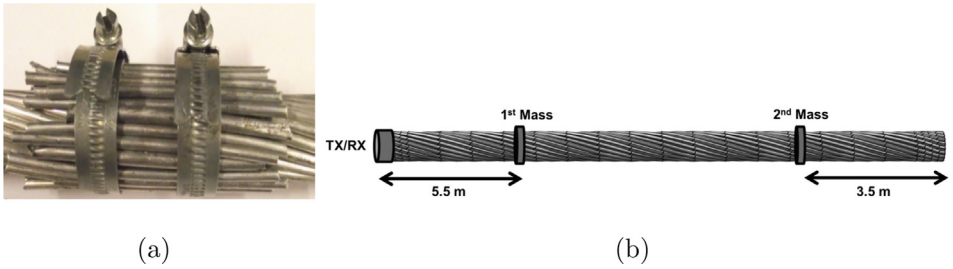

Fig. 9. Photo (a) shows a set of masses (short lengths of wire) attached to the 26.5 m cable. Diagram (b) shows the location these masses relative to the transducer collar for pulse-echo measurements.

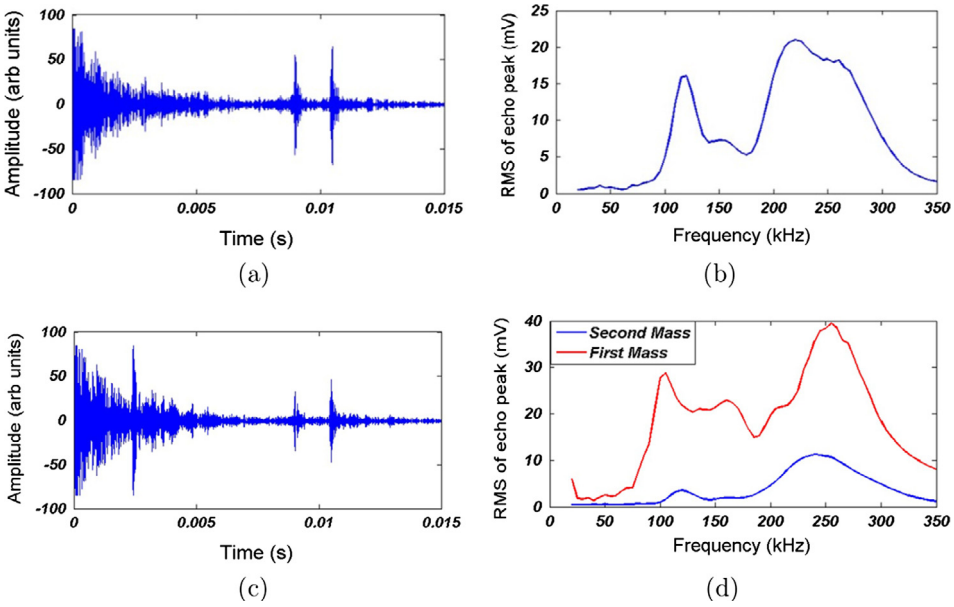

Fig. 10. Graph (a) and (c) show the time domain responses for respectively one mass (220 kHz excitation) and two masses (250 kHz excitation) attached to the cable. Graphs (b) and (d) show the measured reflection echo RMS vs. frequency for respectively one and two masses.

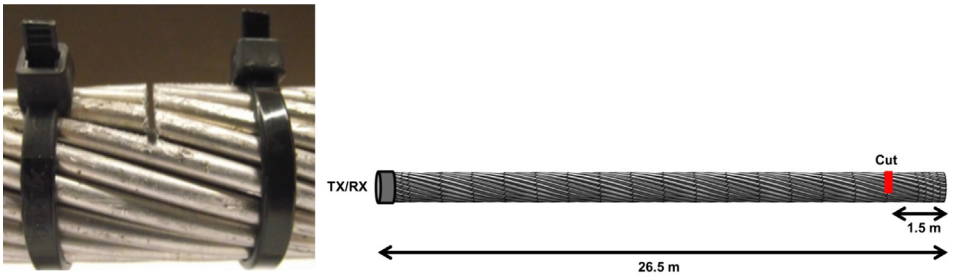

Fig. 11. Photo (a) shows the 6.5 mm deep, 1 mm wide saw cut in the cable and diagram (b) shows the location of the cut.

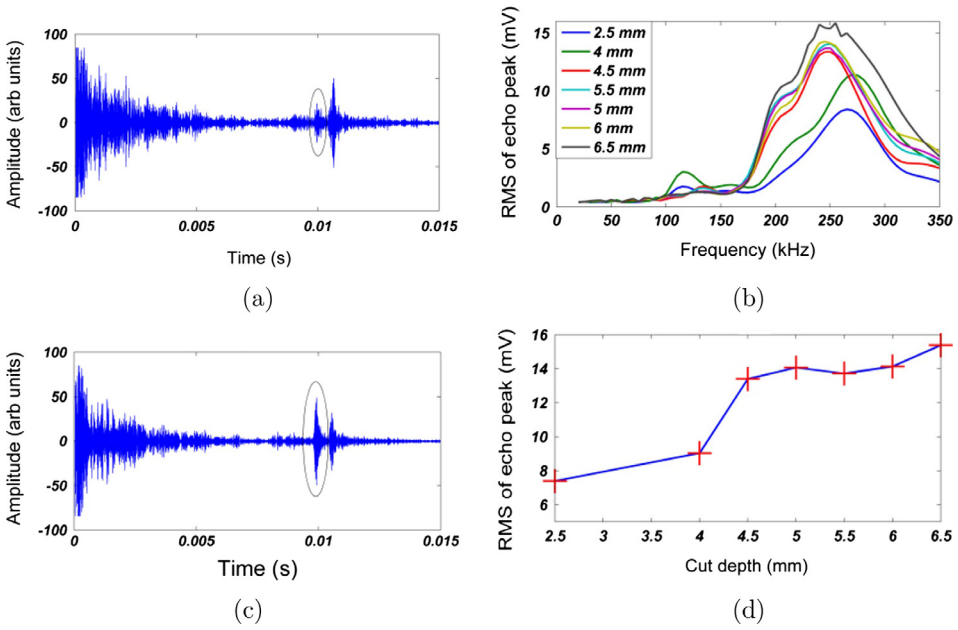

Fig. 12. Graphs (a) and (b) respectively show the 250 kHz excitation response for a 2.5 mm and 6.5 mm deep cut. The defect echoes are circled in these plots. Graph (b) shows the reflection echo RMS vs. frequency for a range of cut depths, while (d) shows the cut depth vs. echo RMS information obtained for 250 kHz excitation.

of 25 m from the transducer collar, as shown in Fig. 11. The cut depth was gradually increased from 2.5 mm to 6.5 mm, which corresponds to approximately 4.5–30.7% reduction in CSA of the cable.

Fig. 12(a) and (c) shows the time domain representations for the 2.5 and 6.5 mm cuts at 250 kHz. The 2.5 mm deep defect (4.5% reduction in CSA) is detected and the 6.5 mm cut (30.7%) is also detectable. Moreover, the resolution of defect detection is less than 1.5 m. Fig. 12(b) indicates that the cut reflection echoes have their peak amplitudes at 250 kHz, which is in line with the results of the previous section. Smaller cut depths, on the other hand, have their amplitude peaks at slightly higher frequencies (260–275 kHz range). Therefore, 250 kHz was chosen as the base frequency for the analysis of the cut depth - echo RMS relationship, which is presented in Fig. 12(d). This plot shows an increase in echo strength with cut depth. The sudden jump in the RMS of the echo shown in Fig. 12(d) for a cut depth greater than 4 mm may be due to the fact that three wires would have been completely cut through at this depth, see Fig. 13.

The variations in the frequencies where defects have their peak values suggest that there is a dependence on defect size and type, a phenomenon that was also apparent in the previous section. This information, although not investigated in this study in depth, could potentially be utilised as features for a more detailed defect characterisation technique. In compliance with the frequency compromises mentioned in this section and the previous section, 250 kHz was decided to be the best frequency for all defect types and sizes for accurate and long range defect detection. However, again it should be noted that this frequency dependence may still be related to the hardware used and should be investigated further in future work.

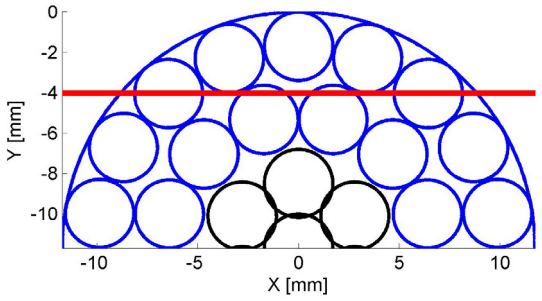

Fig. 13. Plot showing the aluminium and steel wires in the cable. The red line indicates how much of the cable would be cut through for a 4 mm deep cut. (For interpretation of the references to colour in this figure legend, the reader is referred to the web version of this article.)

5. Signal processing

In the previous section, we saw that small defects could be detected in the 26.5 m long cable. However, the received signals had long-duration dead zones and noise. The noise observed in the received signals could be coherent to the transmit signal and may be caused by unwanted reflections caused by the air gaps and non-linear contact between individual wires. Alternatively, the signals can be corrupted with non-coherent noise, such as measurement noise and noise generated by arbitrary sources. Aside from the fact that noise corruption can degrade defect detection quality, it can also reduce inspection range. In order to address the aforementioned problems, wavelet denoising and time scaling techniques are proposed to improve the SNR and inspection range, respectively.

5.1. Wavelet denoising

Wavelet denoising is a popular technique tailored for signals that have a sparse representation in the wavelet domain [7]. This sparsity is exploited in a way that once the original noise-corrupted signal is transformed into the wavelet domain, high-valued wavelet coefficients would correspond to the reflection echo whereas low-valued wavelet coefficients would correspond to the noise. Through applying a suitable threshold value to wavelet coefficients, noise can be eliminated and a purer reflection echo can be reconstructed by applying inverse wavelet transform.

Among many mother wavelets discussed in the signal processing literature, the Daubechies class mother wavelets are reported to have good correlation with ultrasonic reflection echoes of various structures [24,26]. In this study, the mother wavelet was chosen based on its ability to detect the smallest defect (2.5 mm) introduced in the experiments. An empirical analysis yields that the db45 mother wavelet with 5 decomposition levels produces the best results, with hard thresholding scheme and fixed form threshold selection rule. Fig. 14 shows the results obtained using wavelet denoising for the smallest cut depth (2.5 mm) at the peak frequency of 260 kHz.

The wavelet denoising was able to successfully pick up the defect echoes for the two smallest cut depths. The detection of these small defects indicates that the deeper cuts would be detected as well, since these cut echoes would ideally have the same correlation with the chosen mother wavelet (unless the defect geometry or type is different). The smallest cut depth signals are illustration in Fig. 14. In addition to the cases shown in Fig. 14, the abovementioned wavelet denoising parameters managed to detect defects of varying depths and also denoise the signal.

Quantitative analysis of the performance of wavelet denoising was performed using SNR calculations. The SNR was defined for the signal $x(t)$ as [24],

$$SNR_{peak} = \frac{A_{Peak}}{\sigma} \tag{3}$$

where A_{Peak} is the peak amplitude of the echo from the defect and σ is the standard deviation. The signal without deadzone is defined as,

$$x(t) = \begin{cases} 0, & t < \tau \\ x(t \geqslant \tau) & t \geqslant \tau, \end{cases} \tag{4}$$

where τ represents the time limit of the dead zone defined within the time interval $[0,\tau]$. In this study, based on observations made on the raw signals, oscillations up to $\tau = 3$ ms were chosen to be the dead zone and filtered as shown in Eq. (4).

The SNR values are calculated for all cut depths with and without wavelet denoising, and the results are illustrated in Fig. 15(a). For further analysis of wavelet denoising, an Additive White Gaussian Noise (AWGN) based study was conducted. Firstly, the signals acquired from various cut depths were corrupted with various levels of AWGN. Those noise-corrupted signals are then denoised using a wavelet denoising scheme. As the effect of AWGN might not be deterministic, we repeat the "corrupt-then-denoise" procedure a hundred times (once for each cut depth and AWGN level) to achieve a statistically meaningful result. We then analyse the SNR values to assess the success rate of detection. The average SNR values were obtained after repetitive noise corruption and denoising process and the results are illustrated in Fig. 15(b). We lastly devise an SNR threshold value empirically. For the signals that have lower SNR values than the threshold, the technique fails to detect the reflection echo. For the signal that have higher SNR values, the presented technique manages to detect the echoes. This value is also visualised in the said figure (the grey horizontal line) to provide better understanding to the readers.

The wavelet denoising, based on the results shown in Fig. 15(a), consistently improves the SNR values of the signals where the average improvement is around 4–6 dB (around 24% improvement). The results illustrated in Fig. 15(b) indicate that as the noise power increases, defects fall under the noise level and cannot be detected. The small-depth defects fall under the noise level quicker than deep defects and, therefore, they become unresolvable easier (i.e. lower AWGN levels). For instance, the 250 kHz response of the 2.5 mm cut, as shown in Fig. 15(b), can only be detected under the lowest AWGN level (10 dB). Relative to its depth, the 6.5 mm cut can be detected with a higher AWGN level (−5 dB). Fig. 16 shows two representative results of denoising analysis for the 2.5 and 6.5 mm cut depths using 250 kHz excitation. While the wavelet method identifies both the cut and end of the cable in Fig. 16(b) and (d), it can be seen that it struggles to do so for the higher noise level case show in Fig. 16(f).

Fig. 16(b) and (d) have some components that are not filtered but have smaller wavelet coefficients than the defect. Ideally, the threshold value should be as close as possible to the defect's wavelet coefficient so that any component that has a lower coefficient falls under the threshold level and gets filtered. However, manual selection of thresholds with respect to the defect size is not possible since that would require visual identification of the defects and threshold value selection must be done accordingly. In this section,

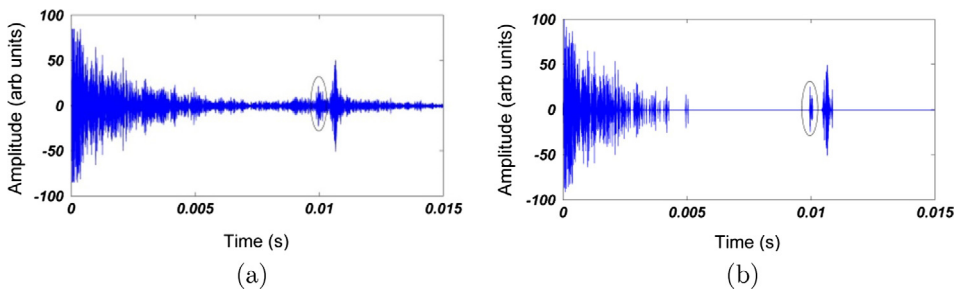

Fig. 14. Graphs show the (a) original and (b) wavelet denoised time traces obtained using 260 kHz excitation signal for the 2.5 mm cut. The echoes corresponding to the defects are circled.

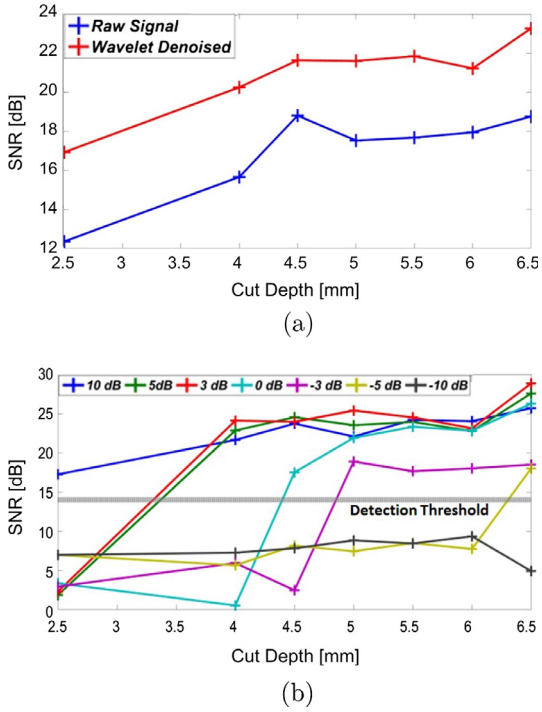

Fig. 15. Graphs show the SNR vs. cut depth for (a) the original signals and (b) the original signals corrupted by various levels of AWGN and then denoised using wavelet denoising. The grey line indicates the detection threshold.

however, the automated technique managed to extract defects and improve the signal SNR accordingly, albeit not as efficiently as a manual threshold selection would have done.

The defects have remained detectable depending on their depth. It should also be kept in mind that in the case of ACSR cables, as mentioned earlier, coherent noise is quite severe. Therefore, additional noise would degrade the signals more severely. Considering the length of the evaluated cable specimen and its respective attenuation, wavelet denoising performed adequately under additive noise.

5.2. Time scaling

The UGW inspection range is often limited by the attenuation that the wave experiences as it propagates through the media. Time-corrected gain, where gain is increased with time, is a convenient way to address the attenuation problem. This, however, is limited by the available hardware.

An alternative approach is to use post processing to scale the received signal to correct for the effects of attenuation [38]. Let $g(t)$ be a received signal sampled at time t. An exponential scaled version of this signal $y(t)$ can be calculated by

$$y(t) = g(t)\, e^{\alpha\, t} \tag{5}$$

where α is a positive constant that needs to be selected with respect to the attenuation experienced by the propagating wave.

The signals should be processed before being scaled to remove DC offset of the signal to prevent this being amplified by the scaling operation. Fig. 17 illustrates the results of the time scaling technique applied on the signal abtained for the 275 kHz excitation and the 4 mm deep cut, where α was set to 260.

In Fig. 17(a), a small echo right after 0.02 s can just be seen. Using the group velocity of the longitudinal wave mode at 275 kHz, this small echo may be identified as the second echo from the cable end. After time scaling, illustrated in Fig. 17(b), the second and third cable end echoes become pronounced.

In Fig. 17(c), the time scaled signal is also denoised using wavelet denoising, using the same parameters as in the previous sections, and a reasonable SNR improvement is visible. It can be seen in this figure that, although time scaling can correct for some effects of attenuation, it also has the effect of exponentially scaling the noise in the signal with time. In any case, seeing the third cable end echo indicates that inspection range is theoretically tripled and an ACSR cable of 78 m length could in fact be inspected with the current hardware. However, it must also be noted that conclusive results with regards to the successful inspection of a 78 m long

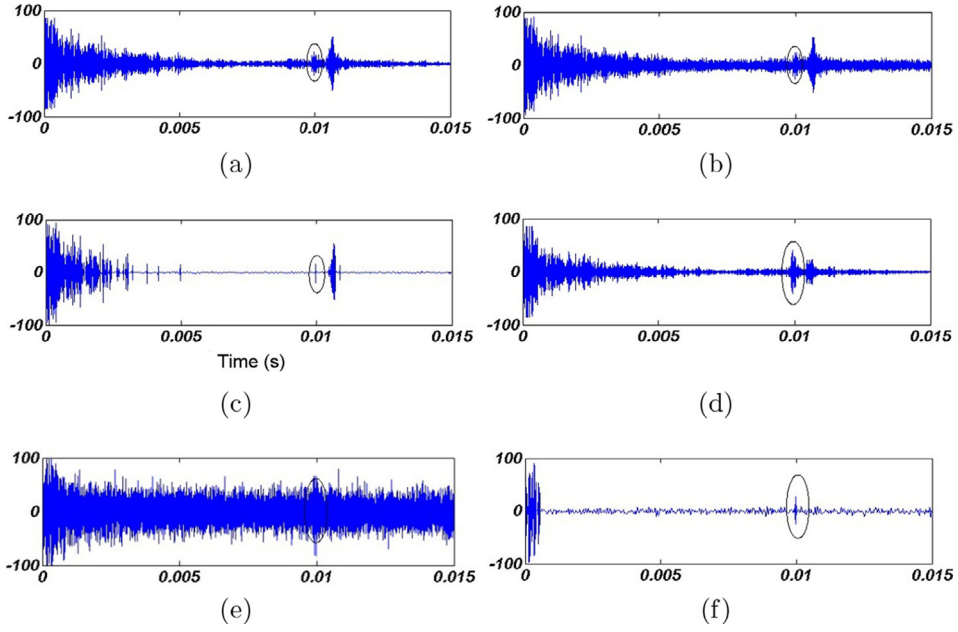

Fig. 16. Graphs showing the time traces obtained for the 2.5 mm deep cut for (a) original, (b) under 10 dB AWGN and (c) under 10 dB AWGN and wavelet denoised. Also shown are the time traces obtained for the 6.5 mm cut for (d) original, (e) under −5 dB AWGN and (f) under −5 dB AWGN and wavelet denoised. The excitation frequency used for both cut depths was 250 kHz.

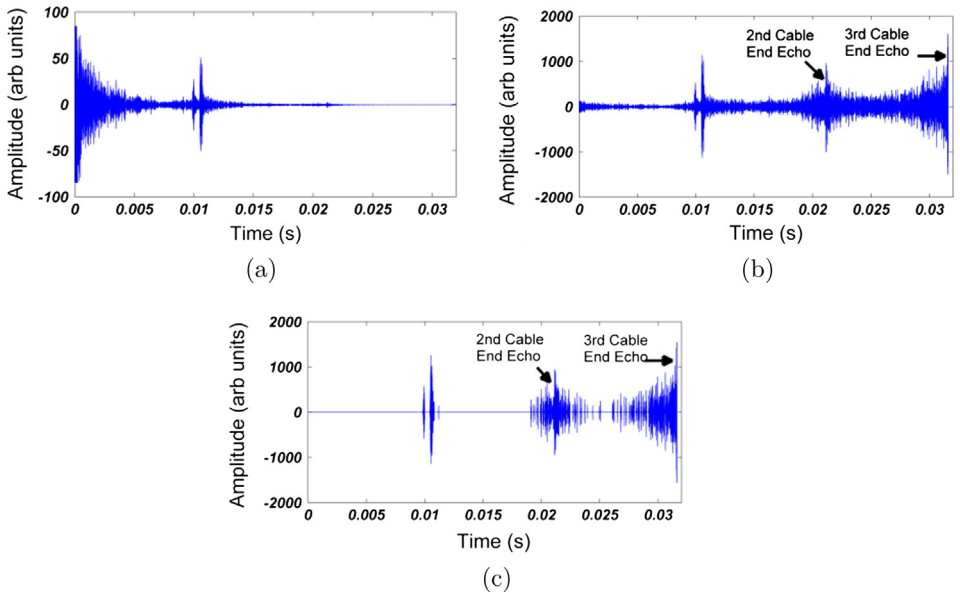

Fig. 17. Graphs show the time traces obtained with 250 kHz excitation and the 4 mm cut for (a) original, (b) time scaled, and (c) time scaled and wavelet denoised.

cable can only be presented after the evaluation of a cable with that length. However, a preliminary framework is laid out here and it can be applied on very long specimens and optimised accordingly.

6. Discussion

This work has been performed using cables which were not under tension and did not have any voltage applied to them. In reality, these cables would be under high tension and be at high voltages. It has been shown that tension can change the wave propagation on multi-wire cables by pushing the strands closer together providing more transfer of ultrasonic energy between wires [4,33,18]. Also, the presence of high voltages will be likely to result in ultrasonic and electrical noise due to corona discharges and vibration. More work is required to investigate ultrasonic guided wave testing for ACSC under these types of real life conditions. In particular, the effect of tension on ultrasonic wave propagation on ACSR cables should be investigated.

7. Conclusion

A new defect detection system that utilises UGW is proposed for inspection of ACSR cables with an aluminium layer inspection emphasis. The wave propagation on an untensioned 2 meter long Bear 325 ACSR cable was studied. Fundamental longitudinal and flexural (and also possibly torsional) wave modes were observed on this shorter length of cable. However, for longer propagation distances (the 26.5 m long cable), only the longitudinal wave mode was observed. Excitation frequencies between 200 and 300 kHz were found to have good concentration of energy in the aluminium layers, and the wave modes present in this frequency band are shown to have similar group velocity dispersion curves with the single-wire aluminium case. However, it should be noted that this frequency response may be related to the specific hardware used. Defect detection using the fundamental longitudinal wave mode at an experimentally identified frequency (250 kHz) managed to detect defects corresponding up to about a 4.5% reduction in CSA for a 26.5 m long ACSR cable. An increase in echo strength with cut depth was observed. Wavelet denoising was applied to the experimental signals and a SNR improvement of up to 24% was achieved. Wavelet denoising under additive noise was analysed and its associated limitations outlined. The time scaling technique was proposed and it successfully managed to increase inspection range approximately up to 78 m. It is also shown that time scaling and wavelet denoising works well together, but optimisation is required. More work is needed to investigate the wave propagation for ACSR cables under tension and at high voltages.

Acknowledgements

The CHAPLIN project is funded by the European Commission under the 7th Framework Programme (FP7) - Research for the benefit of specific groups - Research for SMEs Grant Agreement Number 315130. Chaplin is collaboration between the following organisations: Robotnik Automation S.L.L., Dasel Sistemas S.L, DTK Electronics Ltd., Albatroz Engenharia, TWI Ltd., Innora Robotics and Automatic S.A. and Brunel University. Authors would like to acknowledge Nigel Lee and Makis Livadas for technical guidance.

References

[1] Alleyne DN, Cawley P. A two-dimensional Fourier transform method for the measurement of propagating multimode signals. J Acoust Soc Am 1991;89(3):1159–68.
[2] Azevedo C, Cescon T. Failure analysis of aluminum cable steel reinforced (ACSR) conductor of the transmission line crossing the Parana River. Eng Fail Anal 2002;9(6):645–64.
[3] Baltazar A, Hernandez-Salazar CD, Manzanares-Martinez B. Study of wave propagation in a multiwire cable to determine structural damage. NDT & E Int 2010;43(8):726–32.
[4] Bartoli I, Salamone S, Phillips R, Lanza di Scalea F, Sikorsky CS. Use of interwire ultrasonic leakage to quantify loss of prestress in multiwire tendons. J Eng Mech 2011;137(5):324–33.
[5] Branham SL, Wilson MS, Hurlebaus S, Beadle BM, Gaul L. Nondestructive testing of overhead transmission lines. In: Conference on damage in composite materials. Stuttgart.
[6] Chen G, Wang X, Wang J, Liu J, Zhang T, Tang W. Damage investigation of the aged aluminium cable steel reinforced (ACSR) conductors in a high-voltage transmission line. Eng Fail Anal 2012;19:13–21.
[7] Donoho DL, Johnstone JM. Ideal spatial adaptation by wavelet shrinkage. Biometrika 1994;81(3):425–55.
[8] Gaul L, Sprenger H, Schaal C, Bischoff S. Structural health monitoring of cylindrical structures using guided ultrasonic waves. Acta Mech 2012;223(8):1669–80.
[9] Haag T, Beadle BM, Sprenger H, Gaul L. Wave-based defect detection and interwire friction modeling for overhead transmission lines. Arch Appl Mech 2009;79(6-7):517–28.

[10] Hernandez-Salazar C, Herrejon A, Andara-Sanchez J. Damage detection in multi-wire cables using continuous wavelet transform analysis of ultrasonic guided waves. In: Electronics, robotics and automotive mechanics conference, 2009. CERMA'09. IEEE; 2009. p. 250–5.
[11] Hutchins D, Burrascano P, Davis L, Laureti S, Ricci M. Coded waveforms for optimised air-coupled ultrasonic nondestructive evaluation. Ultrasonics 2014;54(7):1745–59.
[12] International, H.A., 1996–2004. U.S. helicopter summary statistics.
[13] Jiang X, Xinjun W, Liangyun W, Chen H, Yihua K. Detecting the flaws in prestressing strands using guided waves based on the magnetostrictive effect. Insight – Non-Destructive Testing Cond Monit 2007;49(11):647–50.
[14] Kasinathan M, Sosamma S, Pandian C, Vijayakumar V, Chandramouli S, Nashine B, et al. Fiber optic sensors for monitoring sodium circuits and power grid cables. In: 2011 2nd international conference on Advancements in Nuclear Instrumentation Measurement Methods and their Applications (ANIMMA). IEEE; 2011. p. 1–5.
[15] Katrasnik J, Pernus F, Likar B. A survey of mobile robots for distribution power line inspection. IEEE Trans Power Deliv 2010;25(1):485–93.
[16] Kojima Y, Fukuda J, Kumeda T, Iinuma J, Endo M. Corrosion detector robot for overhead transmission line. Fujikura Tech Rev 1992;21:74–83.
[17] Legg M, Yücel M, Kappatos V, Selcuk C, Gan T. Increased range of ultrasonic guided wave testing of overhead transmission line cables using dispersion compensation. Ultrasonics 2015;62:35–45. http://dx.doi.org/10.1016/j.ultras.2015.04.009.
[18] Liu X, Wu B, Qin F, He C, Han Q. Observation of ultrasonic guided wave propagation behaviours in pre-stressed multi-wire structures. Ultrasonics 2017;73:196–205.
[19] Liu Z, Zhao J, Wu B, He C. Temperature dependence of ultrasonic longitudinal guided wave propagation in long range steel strands. Chinese J Mech Eng 2011;24(3):487–94.
[20] Liu Z, Zhao J, Wu B, Zhang Y, He C. Configuration optimization of magnetostrictive transducers for longitudinal guided wave inspection in seven-wire steel strands. NDT & E Int 2010;43(6):484–92.
[21] Marzani A, De Marchi L, Speciale N, Rizzo P. High frequency guided waves in a 7 wire strand: warped frequency transform for spectro-temporal characterization. In: 2009 IEEE International Ultrasonics Symposium (IUS). IEEE; 2009. p. 1503–6.
[22] Mauser S, Rackliffe G, Mousseau Jr T. Investigation of applying new technologies to overhead transmission line inspections, Project 14972; September 1981.
[23] Mudge P. Field application of the Teletest long range ultrasonic testing technique. Insight – Non-Destructive Testing Cond Monit 2001;43(2).
[24] Pardo E, San Emeterio J, Rodriguez M, Ramos A. Noise reduction in ultrasonic NDT using undecimated wavelet transforms. Ultrasonics 2006;44:e1063–7.
[25] Rizzo P. Ultrasonic wave propagation in progressively loaded multi-wire strands. Exp Mech 2006;46(3):297–306.
[26] Rizzo P, di Scalea FL. Ultrasonic inspection of multi-wire steel strands with the aid of the wavelet transform. Smart Mater Struct 2005;14(4):685.
[27] Rizzo P, di Scalea FL. Feature extraction for defect detection in strands by guided ultrasonic waves. Struct Health Monit 2006;5(3):297–308.
[28] Shoemaker TM, Mack JE. The Lineman's and Cableman's Handbook. New York: McGraw-Hill; 2007.
[29] Siegert D, Brevet P. Fatigue of stay cables inside end fittings: high frequencies of wind induced vibrations. Bulletin-Int Organ Study Endurance Ropes 2005;89:43.
[30] Snell J, Renowden J. Improving results of thermographic inspections of electrical transmission and distribution lines. In: ESMO 2000 conference. p. 135–44.
[31] Stix G. Working hot: life at 765 kV. IEEE Spectrum 1988;25(9):54–6.
[32] Sutton J, Lewis K. The detection of internal corrosion in steel reinforced aluminum overhead power line conductors. UK Corrosion, vol. 86. p. 345–59.
[33] Treyssède F. Investigation of the interwire energy transfer of elastic guided waves inside prestressed cables. J Acoust Soc Am 2016;140(1):498–509.
[34] Xingliang J, Xia Y, Hu J, Zhang Z, Shu L, Sun C. An S-transform and support vector machine (SVM)-based online method for diagnosing broken strands in transmission lines. Energies 2011;4(9):1278–300.
[35] Xu J, Tang H, Wu X, Ben A, Kang Y. Broken wire detection in stay cables based on guided waves. In: 2010 international conference on Mechanic Automation and Control Engineering (MACE). IEEE; 2010. p. 1207–10.
[36] Xu J, Xiong H, Wu X. Signal processing for the guided wave test based on the empirical mode decomposition. In: 2011 international conference on Electrical and Control Engineering (ICECE). IEEE; 2011. p. 375–8.
[37] Zhang G-M, Harvey DM. Contemporary ultrasonic signal processing approaches for nondestructive evaluation of multilayered structures. Nondestruct Testing Eval 2012;27(1):1–27.
[38] Zhang X, Sun G, Liu H, Wang Q. Flaw classification in ultrasonic guided waves signal using Wavelet Transform and PNN classifier. In: 2011 international conference on Wireless Communications and Signal Processing (WCSP). p. 1–5.